Case Studies in Construction Materials 18 (2023) e02206

Contents lists available at ScienceDirect

Case Studies in Construction Materials

journal homepage: www.elsevier.com/locate/cscm

Effect of nanomaterials (carbon nanotubes, nano-silica, graphene oxide) on bond behavior between concrete and reinforcing bars

Dongsun Hwangbo [a], Dong-Hee Son [a,*], Heongwon Suh [a], Jaebum Sung [c], Baek-Il Bae [b], Sungchul Bae [a], Hongyun So [c], Chang-Sik Choi [a]

[a] Department of Architectural Engineering, Hanyang University, Seoul, the Republic of Korea
[b] Department of Digital Architecture and Urban Engineering, Hanyang Cyber University, Seoul, the Republic of Korea
[c] Department of Mechanical Convergence Engineering, Hanyang University, Seoul, the Republic of Korea

ARTICLE INFO

Keywords:
Nanomaterials
Dispersion
Reinforced concrete
Bond strength
Bond stress-slip relationship
Volumetric strain

ABSTRACT

The purposes of this study are (i) to evaluate the mechanical properties of triple hybrid-reinforced concrete mixed with carbon nanotubes, nano-silica, and graphene oxide and (ii) to determine the effect of these properties on the bond strength. First of all, compressive strength and splitting tensile strength tests were performed to evaluate the mechanical properties of triple hybrid-reinforced concrete. It has been observed that the flexural strength of concrete increases and the Poisson's ratio and volumetric strain decrease with the incorporation of nano-materials, and the effect is most pronounced when graphene oxide is added. Next, pull-out tests were conducted using a total of 21 specimens of triple hybrid-reinforced concrete. Similarly to the material test results, the bond performance of triple hybrid-reinforced concrete was found to be the highest, which can be attributed to the minimal volumetric deformation of the concrete. By this, the bond strength of Triple hybrid-reinforced concrete was evaluated, taking into account the mechanical properties. When considering Poisson's ratio and flexural strength, it was possible to predict them relatively accurately. In future research, it will be necessary to analyze additional mechanical properties such as friction coefficient and shrinkage strain of nano concrete to incorporate them into the bond strength model.

1. Introduction

Concrete is the most widely used construction material, and research has been conducted to improve the mechanical properties of concrete. Reinforcing concrete with steel fibers is the most commonly used method to improve the mechanical properties of concrete. However, steel fiber reinforced concrete can cause problems such as poor workability and non-uniform fiber dispersion [1–3]. Research on the incorporation of nanomaterials into concrete has recently been conducted to overcome the limitations of steel fiber reinforced concrete [4–8]. The use of nanomaterials as concrete reinforcing materials both improves mechanical properties and maintains workability. Furthermore, the use of nanomaterials as concrete reinforcing materials is increasing due to the recent performance improvement and mass production of nanomaterials [9].

The most widely used nanomaterials are concrete are carbon nanotubes (CNTs), nano-silica (NS), and graphene oxide (GO) [10,11]. CNTs have the advantage of increasing mechanical properties such as the modulus of elasticity of cement composites. In addition, there

* Corresponding author.
E-mail address: son91com@hanyang.ac.kr (D.-H. Son).

https://doi.org/10.1016/j.cscm.2023.e02206
Received 24 March 2023; Received in revised form 25 May 2023; Accepted 7 June 2023
Available online 8 June 2023
2214-5095/© 2023 The Author(s). Published by Elsevier Ltd. This is an open access article under the CC BY license (http://creativecommons.org/licenses/by/4.0/).

are research results that increase the compressive strength, tensile strength, and bending strength of cement composites [12,13]. Additionally, Xu et al. [14] confirmed that crack growth and propagation was prevented due to the bridging effect of CNTs. Second, a pozzolanic reaction occurs and hydration is promoted when NS is mixed with cement [15,16]. As a result, the cement composite becomes denser, and the mechanical properties improved. Finally, GO is a hydrophilic material that has excellent dispersibility when added to an aqueous solution, and its dispersion improves when incorporated with other nanomaterials such as CNTs and NS [17]. This characteristic of GO reduces agglomeration that occurs when nanomaterials are incorporated into an aqueous solution. Therefore, if GO is added when using CNTs and NS, agglomeration should be reduced, and the advantages of CNTs and NS should increase.

Kim et al. [18] investigated the dispersion properties of a triple hybrid solution incorporating CNTs, NS, and GO. Additionally, the mechanical properties of triple hybrid-reinforced cement composite were evaluated. The dispersion of the triple hybrid solution was the highest when GO was incorporated at 0.04 wt % and decreased when GO was incorporated at concentrations higher than 0.04 wt %. In addition, the compressive strength and splitting tensile strength of triple hybrid-reinforced cement composites were the highest when GO was incorporated at 0.04 wt %. On the other hand, the compressive strength and splitting tensile strength decreased when GO was incorporated more than 0.04 wt %. This study confirmed the enhancement of the mechanical properties of the triple hybrid-reinforced cement composite due to the increase in dispersion based on the optimal GO incorporation.

Son et al. [19] conducted research on triple hybrid-reinforced mortar and triple hybrid-reinforced concrete based on Kim et al. [18]. Son et al. [19] proposed a manufacturing and mixing method for concentrated triple hybrid solution, which allows for the batching of a large quantity of nano material solution at once. As shown in Fig. 1, the concentrated triple hybrid solution both increased the amount of deionized water by 9 times, and increased the amount of solutes (nanomaterials) by 4 times during a single ultrasonic dispersion compared to the previous study [18]. Son et al. [19] evaluated the strength of triple hybrid-reinforced mortar and triple hybrid-reinforced concrete using a concentrated triple hybrid solution and triple hybrid solution. As a result, they confirmed that similar strengths were expressed when the concentrated triple hybrid solution and the triple hybrid solution were used. Therefore, this result proved the effectiveness of the concentrated triple hybrid solution.

The reinforcing bar and concrete should act together when designing reinforced concrete members. The bond strength between reinforcing bars and concrete is affected by the mechanical properties of concrete, the concrete cover, and the diameter of the reinforcing bars. Lutz and Gergely [20] defined the three components that constitute the bond and explained the mechanism when reinforcing bar slip occurs. Tepfers [21] calculated the radial force generated by the rib of the reinforcing bar, and a concrete ring model was used. The stresses were calculated in three stages: an elastic stage, a plastic stage, and an elastic stage with internal ring cracks. Esfahani and Rangan [22] proposed a bond strength formula using the tensile strength of high-strength concrete and concrete cover based on the research results of Tepfers [23] and Tilantera and Richard [24]. According to the previous study [25,26], it has been observed that incorporating fibers into concrete to enhance its mechanical properties increases the tensile strength of concrete, consequently leading to an increase in the bond strength between reinforcement and concrete. Therefore, the bond performance is expected to be improved when the mechanical properties are improved by incorporating nanomaterials into concrete and studies on the bond mechanism of nano-reinforced concrete for applying nano-reinforced concrete to structures are increasing.

Wang et al. [27] studied the bond characteristics between plain bar and eight types of nanomaterials and proposed a bond stress-slip relationship model for each nanomaterial. Hassan et al. [28] evaluated the mechanical properties of concrete according to the incorporation of CNTs. Additionally, the effect of CNTs on bond strength was studied through a pull-out test. Hawreen and Bogas [29] conducted a pull-out test to evaluate the bond characteristics between concrete incorporating CNTs and reinforcing bars. Based on the experimental results, scanning electron microscopy confirmed that CNTs delayed the increase in microcrack width. In addition, it was observed that the bonding behavior of steel fibers differs from that of CNTs. Despite controlling only very small microcracks (1 μm), CNTs showed a comparable increase in bond strength to that of steel fibers. In addition, research is being actively conducted to enhance the bond performance between concrete and reinforcing bar using various other nano-materials [30–32].

The bond performance between triple hybrid-reinforced concrete and reinforcing bar should be compared with the bond performance between normal concrete and reinforcing bar. However, there are very few studies on the bond characteristics of triple hybrid-

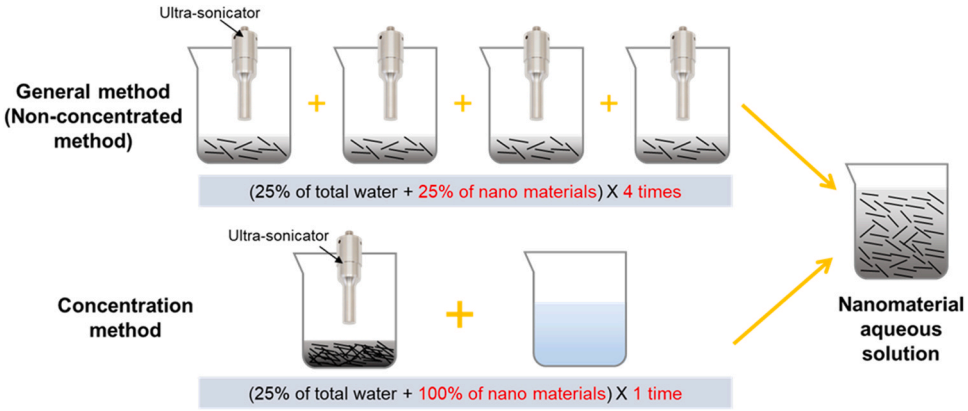

Fig. 1. Concept of nanomaterial aqueous solution manufacturing method [19].

reinforced concrete. Furthermore, until now, the investigation of bond performance in concrete incorporating nanomaterials has predominantly relied on experimental studies, while research on evaluating bond strength using the mechanical properties of novel concrete has been lacking. Therefore, the main purpose of this study is to determine the effect of the mechanical properties of triple hybrid-reinforced concrete on the bond characteristics. In this study, the mechanical properties of triple nano-reinforced concrete with GO incorporation were investigated. Then, the bond characteristics of the triple hybrid-reinforced concrete were evaluated based on the mechanical properties and variables such as GO incorporation, concrete cover thickness, and diameter of reinforcing bars through a pull-out test.

2. Mechanical properties of triple nano-reinforced concrete

2.1. Materials

The mechanical properties of concrete were evaluated based on research conducted by Kim et al. [18]. The dispersion of the triple hybrid solution due to GO incorporation is an important factor in improving the mechanical properties of concrete. Therefore, nanomaterials were incorporated based on the optimal mixing ratio of CNTs, NS, and GO proposed by Kim et al. [18] to confirm the effect of the dispersion of the triple hybrid solution. Therefore, CNTs, NS, and GO were planned to be incorporated at 0.01 wt %, 1 wt %, and 0.04 wt % cement. In addition, concrete mixed with only CNTs and NS were mixed to determine the effect of GO incorporation. The mix proportion of concrete is shown in Table 1 and TEM image of nanomaterials is illustrated in Fig. 2.

The concrete mixing was based on RILEM TC 150-ECM [33]. The concrete mixture starts by adding half of the coarse aggregate and all of the fine aggregate, and then dry mixing for 5 min. Cement is then added, followed by another 30 s of dry mixing, and then the mixing water is introduced. The mixing water consists of tap water and a concentrated solution of nano materials. Afterward, another 30 s of mixing is performed, and the remaining fine and coarse aggregates are added, followed by approximately 5 min of mixing. The concrete was made using type 1 normal Portland cement, coarse aggregate with a size of 25 mm and fine aggregate with a density of 2.6 g/cm^3. A superplasticizer was used to improve the workability of concrete due to the low water-cement ratio. The concrete was mixed using a twin shaft mixer, and the characteristics of the nanomaterials used in mixing are shown in Table 2. The concentrated triple hybrid solution proposed by Son et al. [19] was used because a large amount of the triple hybrid solution is required for triple nano-reinforced concrete mixing.

2.2. Test method

Concrete material testing was conducted for compressive strength and splitting tensile strength. Compressive strength and splitting tensile strength were performed using specimens with a size of Φ100 × 200 mm. The machine used for the strength test is a universal testing machine with a capacity of 1000 kN. Additionally, all strength tests were performed according to KS F 2405 [34] and KS F 2423 [35]. The material test setup is depicted in Fig. 3.

All specimens were tested after a curing period of at least 28 days. To enhance the reliability of the material test results, compressive and splitting tensile strengths were tested using about 5–6 separate batches on different dates. The total number of specimens tested for each mix proportion was more than 30. To measure the strain of the specimens during the test, strain gauges were attached in the vertical direction to the top, middle, and bottom three positions, and strain gauges were also attached in the horizontal direction to the center of the specimen during the compressive strength test.

2.3. Test results

Table 3 is showing the concrete strength test results. First, the compressive strength (f_c') of 0GCS was 84.10 MPa, an increase of about 2.5 % compared to OPC. In addition, f_c' of 0.04GS was 84.18 MPa, an increase of about 2.6 % compared to OPC. Second, splitting tensile strength (f_{sp}) of 0GCS was 5.17 MPa, an increase of about 23.1 % compared to OPC. On the other hand, the f_{sp} of 0.04 GCS was 5.5 MPa. This result is an increase of about 31.0 % compared to OPC and a 6.4 % increase compared to 0GCS. Therefore, strength tests were used to confirm that the increase in f_c' when incorporating nanomaterials was insignificant, but the increase in f_{sp} was significant.

Since Poisson's ratio (ν_c) and volumetric strain of concrete (ε_{vol}) are important factors in evaluating the nonlinear behavior of concrete, the horizontal strains of concrete (ε_h) were evaluated. The evaluation of the Poisson's ratio was conducted with reference to KS F 2438 [36]. Values of ν_c by concrete types OPC, 0GCS, and 0.04GCS were 0.23, 0.24, and 0.21, respectively. Comparing the results,

Table 1
Mix proportions of concrete.

Type	W/C	W (kg/m^3)	C (kg/m^3)	CA (kg/m^3)	FA (kg/m^3)	SP (wt %)	CNTs (wt %)	NS (wt %)	GO (wt %)
OPC	0.22	165	739	960	618	0.7	—	–	–
0GCS							0.01	1	–
0.04GCS							0.01	1	0.04

W: water, C: cement, CA: coarse aggregate, FA: fine aggregate, SP: superplasticizer.
The unit wt % is with respect to the weight of cement.

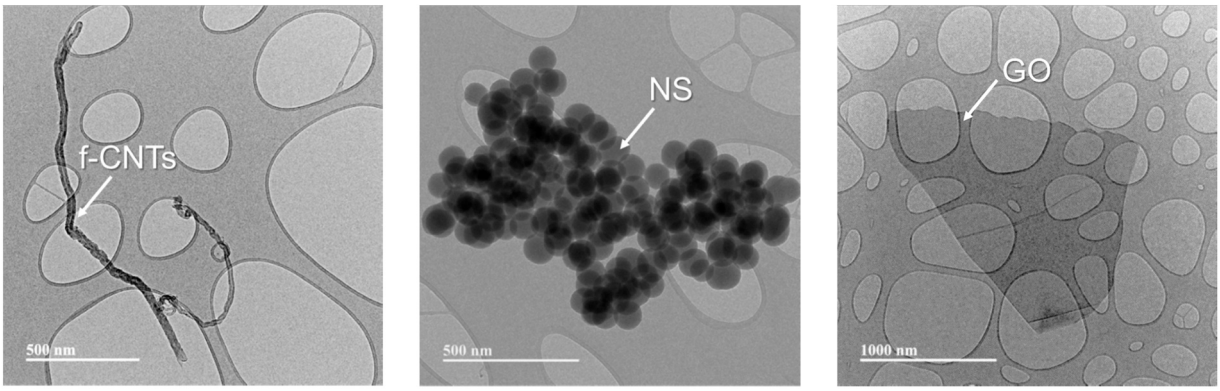

(a) Functionalized carbon nanotube (b) Nano-silica (c) Graphene Oxide

Fig. 2. TEM image of nanomaterials.

Table 2
Physical properties of nanomaterials.

Nanomaterials	Purity (wt %)	Specific surface area (m^2/g)	Diameter (mm)	Length (μm)	Average particle size (nm)	Thickness (nm)	Layer diameter (μm)
CNTs	95	> 200	5–15	10–30	–	–	–
NS	99.9	> 23	–	–	110	–	–
GO	> 98	–	–	–	–	~1	0.2–10

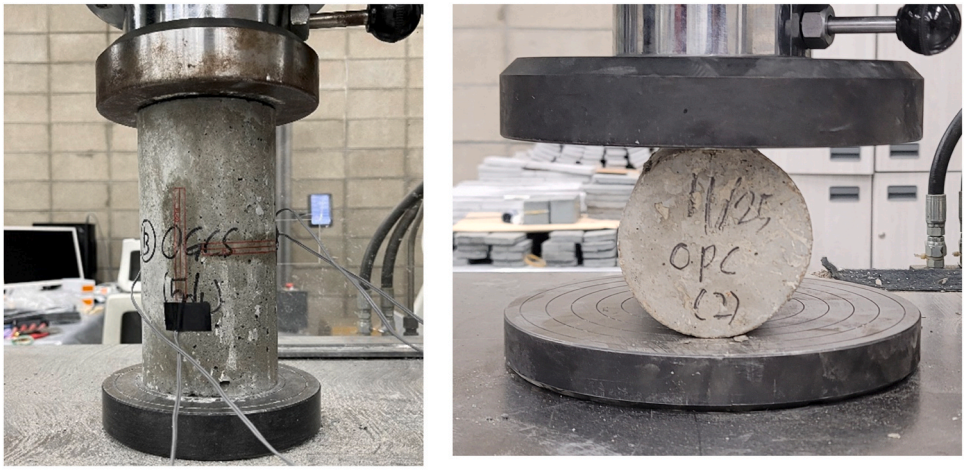

(a) Compressive strength test (b) Splitting tensile strength test

Fig. 3. Concrete strength tests.

Table 3
Mechanical properties of concrete with nanomaterials.

Type	f_c' (MPa)	ε_0 (mm/mm)	E_c (MPa)	υ_c	f_{sp} (MPa)
OPC	82.04	0.00270	32,845	0.23	4.20
0GCS	84.10	0.00262	34,905	0.24	5.17
0.04GCS	84.18	0.00267	35,272	0.21	5.50

f_c': compressive strength of concrete, ε_0: strain at peak stress of concrete, E_c: elastic modulus of concrete, υ_c: Poisson's ratio of concrete, f_{sp}: splitting tensile strength of concrete.

0.04GCS is about 12.5 % smaller than 0GCS. This means that ε_h of 0.04GCS occurs less than ε_h of 0GCS under the same axial load. The second is a comparison of ε_{vol} by concrete type. The stress-strain curve and ε_{vol} for each concrete type are shown in Fig. 4. ε_{vol} was obtained as the sum of twice ε_h and the vertical strain (ε_h) as shown in Eq. (1).

$$\varepsilon_{vol} = \varepsilon_v + 2\varepsilon_h \tag{1}$$

For an ε_{vol} comparison, specimens with the same secant modulus were used for each concrete type. As a result, ε_{vol} was the smallest at 0.04GCS and the largest at OPC. In addition, 0GCS and 0.04GCS decreased by about 17.3 % and about 33.7 % compared to OPC. In conclusion, strength test results confirmed that the incorporation of GO increased f_{sp} and reduced the dilation in uniaxial compression. The reason is that GO doping enhances the dispersibility of nanomaterials, preventing agglomeration and reducing porosity, while also promoting the hydration reaction [18,19].

3. Pull-out test of triple nano-reinforced concrete

3.1. Test plan

Bond stress is affected by various factors such as concrete cover thickness (c_s), embedded length of reinforcing bar (l_d), and the diameter of the reinforcing bar (d_b) [37–40]. In this study, a pull-out test was performed to evaluate various factors affecting the bond characteristics of triple nano-reinforced concrete and to identify the bond mechanism. The main purpose of this study was to evaluate the effect of GO incorporation on the mechanical properties of triple nano-reinforced concrete on the bond characteristics. Furthermore, in ACI 318-19 [41], when calculating the development length (l_d) of the rebar, the diameter of the rebar and the concrete cover thickness are required according to Eq. (2), without considering the material strength. Therefore, the variables of the pull-out test specimen are the amount of nanomaterial, c_s, l_d, and d_b.

$$l_d = \frac{f_y}{1.1\lambda\sqrt{f'_c}} \frac{\Psi_t\Psi_e\Psi_s\Psi_g}{\left(\frac{c_b+K_{tr}}{d_b}\right)} d_b \tag{2}$$

Here, λ is the modification factor to reflect the lightweight concrete, ψ_t, ψ_e, ψ_s, ψ_g are the factor used to modify development length, K_{tr} is the transverse reinforcement index.

A specimen was fabricated using the concrete mix proportion in Table 1 to confirm the bond stress as a function of GO incorporation. The specimen induced pull-out failure and splitting failure, and the failure mode is affected by l_d. According to Tepfers [21], when tensile stress is applied to reinforcing bars embedded in concrete, the radial stress determined by embedded length is applied to

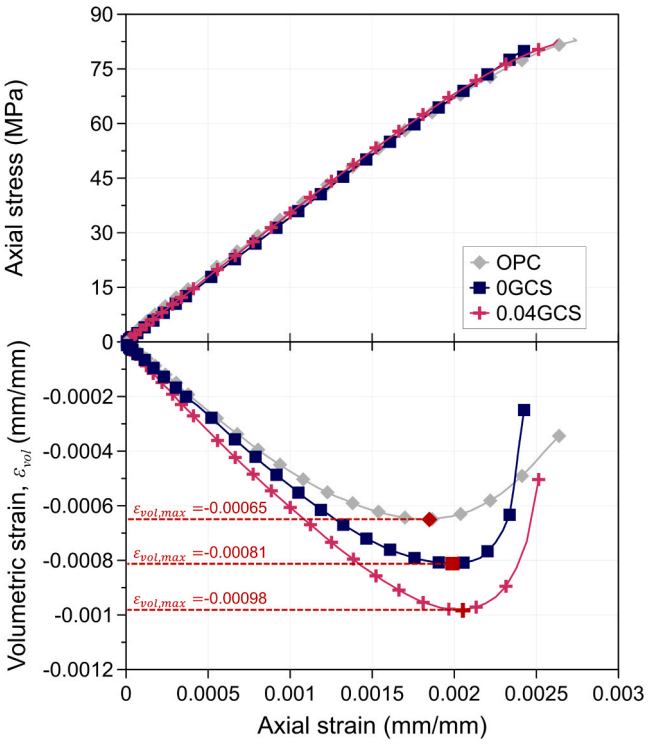

Fig. 4. Stress-strain relationship of concrete with nanomaterials.

the concrete. If this stress is higher than the tensile strength of the concrete, splitting failure will occur. When the embedded length is short, pull-out failure occurs because the radial stress is low. Conversely, when the embedded length is long, splitting failure occurs. In this study, the l_d of the D16 reinforcing bar was set to $1.5d_b$ to induce pull-out failure, and l_d was set to $3d_b$ to induce splitting failure. In RILEM RC6 [42], which was referred to when fabricating the specimen, l_d is suggested as $5d_b$. However, for specimens with high strengths above 70 MPa, the reinforcing bar may yield before concrete failure. To prevent this, l_d was set to $3d_b$ or less.

In addition, c_s and d_b, which affect splitting failure, were set as variables. There are three types of d_b: D13, D16, and D22. c_s was set according to RILEM RC6 [42] and KDS 14 20 52 [43]. The test specimen designations followed the convention shown in Fig. 5. When fabricating the specimen, PVC pipes were used to generate bond stress only where the reinforcing bar was embedded. The test specimen details are shown in Fig. 6.

A total of 21 specimens were planned, and the specifications of each specimen and the material test results for each concrete mix proportion are presented in Table 4. The specimens were produced on different dates, and due to the limited capacity of the shaft mixer, the pull-out test specimens and the specimens for material testing were produced in two separate batches. The concrete strengths presented in Table 4 are the material test results of the specimens produced simultaneously with the pull-out test specimens, which differ from those in Table 3. The nominal yield strength of the reinforcing bars used in this study was 500 MPa. The tensile strength test results of reinforcing bars according to KS B 0802 [44] all showed results exceeding the nominal yield strength. The tensile strength test results of reinforcing bar are shown in Table 5.

3.2. Test procedure

Fig. 7 shows the test setup. A screw jack with a capacity of 500 kN was used to pull out the reinforcing bar. Additionally, a coupler was installed at the end of the reinforcing bar to fix the reinforcing bar during the test. Teflon plates were placed to minimize friction between the frame and the bottom and side surfaces of the specimen. Specimens were tested using a displacement control system and were controlled at a rate of 0.5 mm/min.

The slip between the concrete and the reinforcing bar that occurred during the test was measured using a linear-variable displacement transducer (LVDT). The relative displacement between the free end of the reinforcing bar and the concrete and the eccentricity of the specimen were measured through LVDT 3 and LVDT 4. In addition, six LVDTs were additionally installed to measure the movement and eccentricity of the frame that occurred during the test.

3.3. Test results

3.3.1. Failure modes

The pull-out test results are shown in Table 6. The actual bond stress applied to the reinforcing bar was distributed differently for each position of the reinforcing bar. However, it is impossible to determine the load based on the position of the reinforcing bar. Assuming that the load acting on l_d is equal, the average bond stress (τ) between the reinforcing bar and the concrete was obtained as shown in Eq. (3).

$$\tau = \frac{F}{\pi d_b l_d} \tag{3}$$

where F is tensile force on reinforcing bar.

Pull-out failure occurred in all specimens with an l_d of $1.5d_b$, and the typical crack patterns at failure are shown in Fig. 8(a). On the other hand, all specimens with l_d of $3d_b$ and a thin concrete cover of $3.1c_s/d_b$ or less had splitting failure. The specimens with a thin concrete cover have cracks on the side of the specimen, and the typical crack patterns at failure are shown in Fig. 8(b).

Three failure modes occurred in the specimen with an l_d of $3d_b$ and a thick concrete cover of $4.5c_s/d_b$ or more. The specimens with D13 reinforcing bar diameter showed two failure modes: splitting failure and pull-out failure. Splitting failure was observed in 0GCS-D13-7.4C-3L, however pull-out failure was observed in OPC-D13-7.4C-3L and 0.04GCS-D13-7.4C-3L. The reason for this is that the absolute values of f_c' and f_{sp} for 0GCS are greater than OPC and 0.04, suggesting that yielding of the reinforcing bar occurs at the bond length of $3d_b$ when a sufficient cover thickness is provided. Additionally, variations in the failure patterns can occur even within the same experiment in bond tests, leading to the conclusion that such phenomena have been observed [45,46].

Second, splitting failure and reinforcing bar yielding occurred in the specimens with a D16 reinforcing bar diameter. Splitting failure was observed in OPC-D16-5.8C-3L and 0.04GCS-D16-5.8C-3L. However, in 0GCS-D16-5.8C-3L, the reinforcing bar yielded before failure, thus the exact bond strength could not be determined. This is because f_c' and f_{sp} of 0GCS are relatively higher than those of OPC and 0.04GCS.

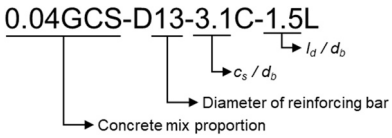

Fig. 5. Bond specimen designation.

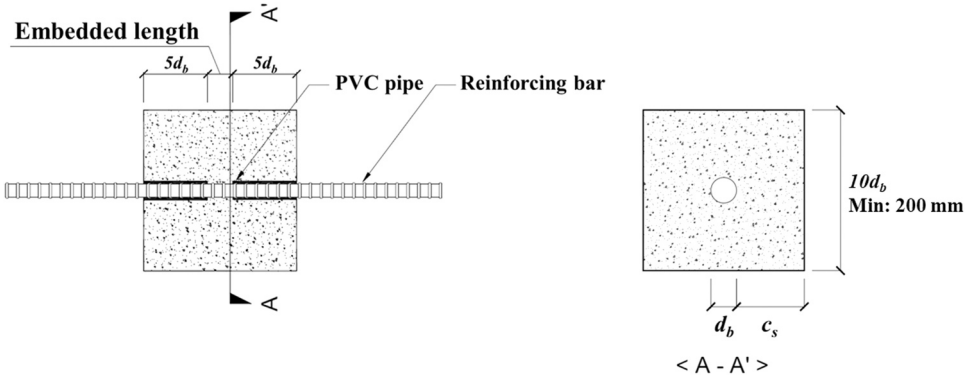

Fig. 6. Test specimen details.

Table 4
Details of test specimens.

No.	Specimen	Concrete designation	f_c' (MPa)	f_{sp} (MPa)	c_s/d_b	l_d/d_b	Reinforcing bar designation	Predicted failure mode
1	OPC-D16-5.8C-1.5L	OPC	82.68	5.10	5.8	1.5	D16	Pull-out
2	0GCS-D16-5.8C-1.5L	0GCS	87.38	5.85				
3	0.04GCS-D16-5.8C-1.5L	0.04GCS	79.64	4.38				
4	OPC-D13-7.4C-3L	OPC	82.68	5.10	7.4	3	D13	Splitting
5	0GCS-D13-7.4C-3L	0GCS	87.38	5.85				
6	0.04GCS-D13-7.4C-3L	0.04GCS	79.64	4.38				
7	OPC-D13-3.1C-3L	OPC	82.68	5.10	3.1			
8	0GCS-D13-3.1C-3L	0GCS	87.38	5.85				
9	0.04GCS-D13-3.1C-3L	0.04GCS	82.09	5.94				
10	OPC-D16-5.8C-3L	OPC	82.68	5.10	5.8		D16	
11	0GCS-D16-5.8C-3L	0GCS	87.38	5.85				
12	0.04GCS-D16-5.8C-3L	0.04GCS	79.64	4.38				
13	OPC-D16-2.5C-3L	OPC	82.68	5.10	2.5			
14	0GCS-D16-2.5C-3L	0GCS	87.38	5.85				
15	0.04GCS-D16-2.5C-3L	0.04GCS	79.64	4.38				
16	OPC-D22-4.5C-3L	OPC	77.76	5.33	4.5		D22	
17	0GCS-D22-4.5C-3L	0GCS	85.57	5.54				
18	0.04GCS-D22-4.5C-3L	0.04GCS	75.50	4.99				
19	OPC-D22-1.8C-3L	OPC	77.76	5.33	1.8			
20	0GCS-D22-1.8C-3L	0GCS	85.57	5.54				
21	0.04GCS-D22-1.8C-3L	0.04GCS	75.50	4.99				

c_s: the concrete cover thickness, l_d: the embedded length of reinforcing bar, d_b: diameter of the reinforcing bar.

Table 5
Mechanical properties of reinforcing bars.

Reinforcing bar designation	d_b (mm)	f_y (MPa)	f_{ym} (MPa)	f_u (MPa)	ε_y (mm/mm)
D13	12.7	500	559.9	632.6	0.0028
D16	15.6		550.1	674.4	0.0028
D22	22.2		541.4	720.5	0.0027

f_y: nominal yield strength of reinforcing bar, f_{ym}: measured yield strength of reinforcing bar, f_u: tensile strength of reinforcing bar, ε_y: yield strain of reinforcing bar.

Finally, splitting failure was observed in OPC-D22-4.5C-3L, 0GCS-D22-4.5C-3L, and 0.04GCS-D22-4.5C-3L using a D22 reinforcing bar diameter. This is because the specimens used a thick reinforcing bar with a diameter of 22.2 mm. In addition, the concrete cover of the specimens was 4.5c_s/d_b, and they had a thinner concrete cover than the specimens using D13 and D16 reinforcing bar diameter.

3.3.2. Bond stress-slip curve

A bond stress-slip curve is proposed in the *fib* Model Code 2010 [47]. This equation goes up to $\tau_{b,\max}$ and is given in Eq. (4).

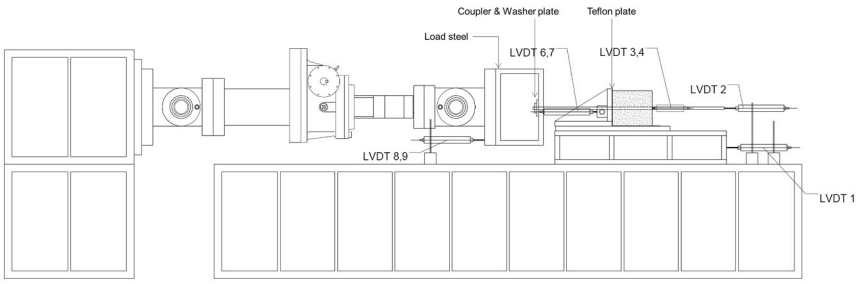

(a) Front view

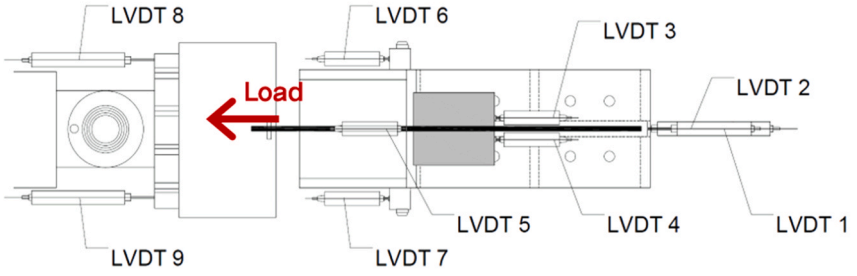

(b) Top view

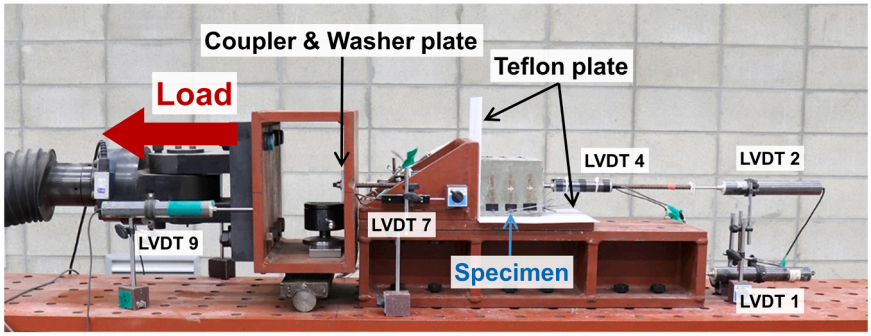

(c) Test setup photograph

Fig. 7. Test setup for pull-out test.

$$\tau_b = \tau_{b,\max}\left(\frac{s}{s_1}\right)^{\alpha} (0 \le s \le s_1) \tag{4}$$

Here, τ_b is bond stress, s is the slip between reinforcing bar and concrete, s_1 is the slip at the maximum bond stress, and α is a coefficient.

Fig. 9 shows the bond stress-slip curve of the specimen that induced pull-out failure. In the bond stress-slip curve, the change in the ascending curve according to the incorporation of nanomaterials was evaluated. To compare slip reaching $P_{\max}$, τ_b was divided by $\tau_{b,\max}$. Based on Eq. (4), $s_{free\ \ end}$ was divided by s_1 to compare the slip up to $\tau_b/\tau_{b,\max}$. $s_{free\ \ end}$ was calculated as the average of LVDT 3 and LVDT 4.

The bond stress-slip curve between reinforcing bars and concrete can be modeled based on α [38], and smaller values of α are related to smaller slip at the same τ_b. To derive the value of α for each test specimen, linear regression analysis should be performed based on normalized data. By dividing both sides of Eq. (4) by $\tau_{b,\max}$ and taking the natural logarithm, it can be expressed as $\ln\left(\frac{\tau_b}{\tau_{b,\max}}\right) = \alpha\ln(\frac{s}{s1})$, as shown in Eq. (5). Following Eq. (5), performing linear regression analysis with $\ln\left(\frac{\tau_b}{\tau_{b,\max}}\right)$ as the dependent variable and $\ln\left(\frac{s}{s1}\right)$ as the independent variable, while fixing the y-intercept to 0, allows us to obtain the slope through linear regression analysis. This slope represents α in Eq. (5).

$$\ln\left(\frac{\tau_b}{\tau_{b,\max}}\right) = \alpha\ln(\frac{s}{s1})(0 \le s \le s_1) \tag{5}$$

α of 0.04GCS-D16-5.8C-1.5L was the smallest at 0.22, whereas α of 0GCS-D16-5.8C-1.5L was the largest at 0.56. Although $f_c{}'$ and f_{sp}

Table 6
Test results.

No.	Specimen	P_{max} (kN)	$\tau_{b,max}$ (MPa)	$\frac{\tau_{b,max}}{f_{sp}}$	$s_{free\ end}$ (mm)	Actual failure mode
1	OPC-D16-5.8C-1.5L	77.13	67.26	13.18	0.678	Pull-out
2	0GCS-D16-5.8C-1.5L	70.17	61.19	10.47	0.937	Pull-out
3	0.04GCS-D16-5.8C-1.5L	36.78	32.07	6.72	0.246	Pull-out
4	OPC-D13-7.4C-3L	66.67	43.86	8.59	0.788	Pull-out
5	0GCS-D13-7.4C-3L	71.79	47.23	8.08	0.379	Splitting
6	0.04GCS-D13-7.4C-3L	67.71	44.54	9.33	0.626	Pull-out
7	OPC-D13-3.1C-3L	43.08	28.34	5.55	0.047	Splitting
8	0GCS-D13-3.1C-3L	38.29	25.19	4.31	0.038	Splitting
9	0.04GCS-D13-3.1C-3L	52.48	34.52	5.81	0.214	Splitting
10	OPC-D16-5.8C-3L	99.85	43.53	8.53	0.356	Splitting
11	0GCS-D16-5.8C-3L	128.3	55.94	9.57	4.089	Reinforcing bar yielding
12	0.04GCS-D16-5.8C-3L	108.17	47.16	9.88	0.772	Splitting
13	OPC-D16-2.5C-3L	67.51	29.43	5.77	0.168	Splitting
14	0GCS-D16-2.5C-3L	60.75	26.49	4.53	0.046	Splitting
15	0.04GCS-D16-2.5C-3L	59.00	25.72	5.39	0.166	Splitting
16	OPC-D22-4.5C-3L	142.05	30.58	5.74	1.180	Splitting
17	0GCS-D22-4.5C-3L	96.79	20.84	3.76	0.045	Splitting
18	0.04GCS-D22-4.5C-3L	153.3	33.00	6.62	0.201	Splitting
19	OPC-D22-1.8C-3L	127.78	27.51	5.16	0.176	Splitting
20	0GCS-D22-1.8C-3L	114.51	24.65	4.45	0.067	Splitting
21	0.04GCS-D22-1.8C-3L	98.62	21.23	4.26	0.143	Splitting

P_{max}: maximum load, $\tau_{b,max}$: maximum bond strength, $s_{free\ \ end}$: free end slip at maximum load.

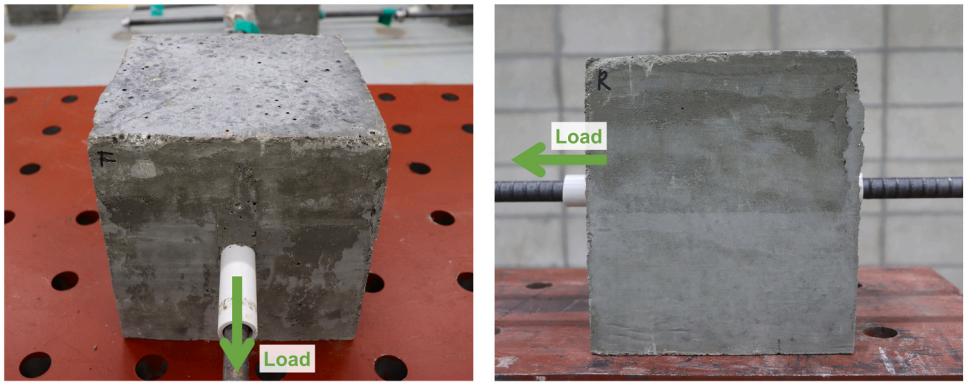

(a) Pull-out failure

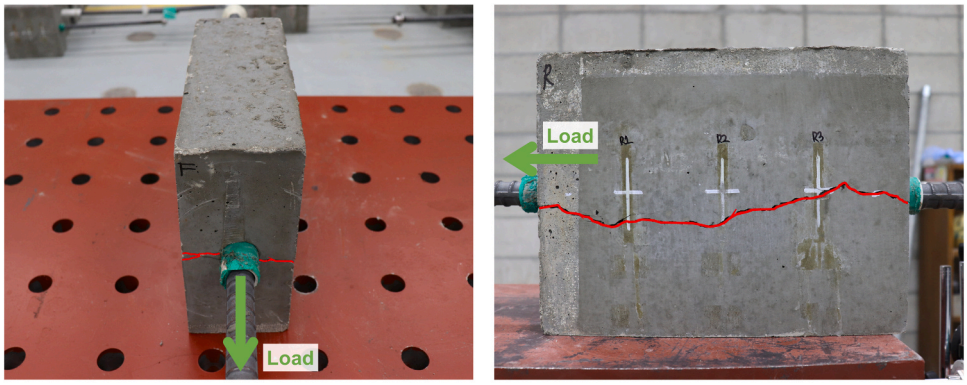

(b) Splitting failure of specimen with thin concrete cover

Fig. 8. Typical crack patterns at failure.

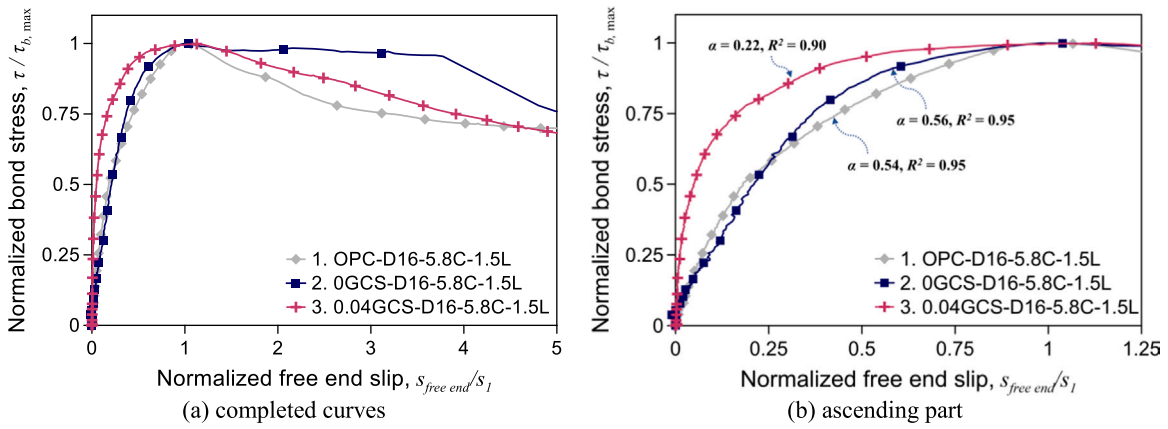

Fig. 9. Effect of nanomaterials on the normalized bond stress-slip curves.

values of 0.04GCS-D16-5.8C-1.5L were the smallest, α was the smallest. In conclusion, slip is reduced at the same bond stress when GO is incorporated.

3.3.3. *Effect of concrete cover*

The bond strength between the concrete and the reinforcing bar is affected by f_{sp}. In this study, the effect of f_{sp} was eliminated by dividing $\tau_{b,max}$ by f_{sp}. Specimens in which splitting failure was observed were affected by d_b and c_s. Therefore, normalized bond stress ($\tau_{b,max}/f_{sp}$) according to c_s/d_b was evaluated for the specimens in which splitting failure was observed. This result is shown in Fig. 10. In addition, the regression analysis formula results are shown in Table 7.

Among the specimens with the same c_s/d_b, 0.04GCS had the largest $\tau_{b,max}/f_{sp}$ except for the specimen with $1.8c_s/d_b$. The rate of increase of $\tau_{b,max}/f_{sp}$ with growing c_s/d_b increased in the order of OPC, 0GCS, and 0.04GCS. This result is due to the high dispersion of incorporated GO. In addition to f_{sp}, the changes in mechanical properties of concrete as a function of GO incorporation affected the bond strength.

3.3.4. *Strain distribution*

v_c and ε_{vol} affect the strain generated in the specimen during the pull-out test. Therefore, strain (ε) was measured during the pull-out test to investigate the effect of the mechanical properties of concrete on the bond strength. To accurately measure ε, a strain gauge was attached to the specimen with a concrete cover of $3.1c_s/d_b$ or less, which is expected to crack on the lateral face of the specimen. Strain gauges were attached to the lateral face of the specimen with the same spacing, and the location of the strain gauge is shown in Fig. 11. Strain gauges were named G1, G2, and G3 in order starting closest to the loaded end.

Fig. 12 shows ε of the specimen at P_{max}. There was no significant difference in ε of G3 for all specimens. However, ε of G1 was the smallest for the specimen made of 0.04GCS concrete regardless of c_s/d_b.

Fig. 13 shows the lateral strain at G1 (ε_{G1}) according to c_s/d_b. A smaller c_s/d_b yields a larger strain difference. The specimen made of 0.04GCS had the smallest ε_{G1} compared to other specimens, and 0.04GCS-D22-1.8C-3L had about 76 % lower ε_{G1} than OPC-D22-1.8C-3L. These results are also influenced by the mechanical performance of 0.04GCS, which has a smaller v_c and ε_{vol} compared to

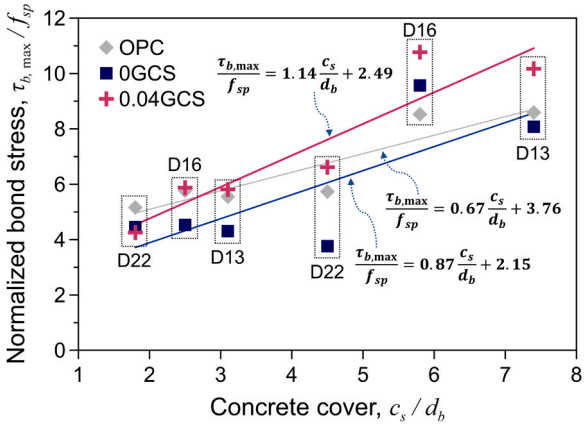

Fig. 10. Effect of concrete cover on the normalized bond strength.

Table 7
Regression analysis formula results of bond strength.

Type	Regression analysis formula	R^2
OPC	$\frac{\tau_{b,\max}}{f_{sp}} = 0.67\frac{c_s}{d_b} + 3.76$	0.83
0GCS	$\frac{\tau_{b,\max}}{f_{sp}} = 0.87\frac{c_s}{d_b} + 2.15$	0.59
0.04GCS	$\frac{\tau_{b,\max}}{f_{sp}} = 1.14\frac{c_s}{d_b} + 2.49$	0.86

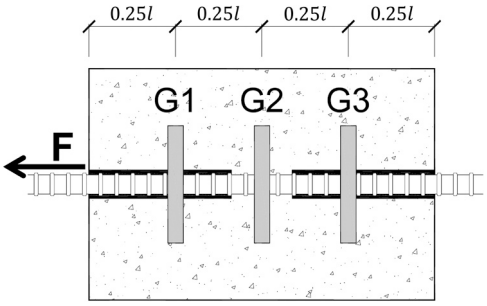

Fig. 11. Strain gauge locations for test specimens.

OPC and 0GCS, regardless of f_c' and f_{sp}. According to previous studies [29], it has been reported that carbon nanotubes (CNTs) effectively control microcracks, leading to improved adhesion performance. Additionally, the incorporation of graphene oxide (GO) enhances the dispersion of nanomaterials and prevents agglomeration [18,19]. It is believed that the increased dispersion of CNTs due to the incorporation of GO promotes crack control through cross-linking effects in concrete.

4. Evaluation of bond strength

The pull-out test of triple hybrid-reinforced concrete showed that the bond characteristics are affected by f_{sp} and ε_{vol}. As a result of the concrete strength test, f_{sp} increased, and the dilation was reduced according to GO incorporation. In the evaluation of bond characteristics through the pull-out test, $\tau_{b,\max}/f_{sp}$ increased and $s_{free\ \ end}$ decreased as the transverse strain of concrete against radial stress decreased. Therefore, when calculating τ_b of triple hybrid-reinforced concrete, it is important to consider the mechanical properties f_{sp} and ν_c, which is closely related to the volumetric deformation of concrete.

According to Lutz and Gergely [20], bonds consist of three components: chemical adhesion, friction, and mechanical interaction between concrete and steel. In the initial loading, chemical adhesion and mechanical interaction reduce the slip of the reinforcing bar. Slip occurs after the chemical adhesion is lost. Slip can be prevented due to the bearing force between the rib of the reinforcing bar and the concrete. Rehm [48] and Lutz [49] performed pull-out tests using reinforcing bars with rib face angles between 40° and 105°. If the angle of the rib face is greater than 40–45°, friction should be considered because the friction between the rib face and the concrete effectively prevents slip of the reinforcing bar. Since the angle of the rib face of the reinforcing bar used in this study is greater than 45° according to KS D 3504 [50], friction should be considered when calculating the bond strength.

Hu et al. [51] proposed a formula for splitting bond strength as the sum of mechanical interaction and friction. For the mechanical interaction calculation formula, the formula proposed by Tepfers [21] was used when the concrete was partly cracked. The friction equations proposed by Timoshenko and Goodier [52] and Bathe and Chaudhary [53] were used.

The splitting bond strength (τ_{sp}) can be expressed as Eq. (6).

$$\tau_{sp} = \tau_m + \tau_f + \tau_c \tag{6}$$

where τ_m is mechanical interaction, τ_f is friction, and τ_c is chemical adhesion.

τ_c resists only small loads and has little effect on bond strength. Therefore, it is assumed that there is no chemical adhesion when calculating bond strength. According to Tepfers [21], when partial cracks occur in concrete, τ_m is calculated as in Eq. (7).

$$\tau_m = f_{ct}\frac{c_s + R_s}{1.664 d_b} \tag{7}$$

where f_{ct} is tensile strength of concrete, and R_S is the radius of the reinforcing bar, $d_b/2$.

Hu et al. [51] expressed τ_f as shown in Eq. (8) based on the radial stress calculation equation proposed by Timoshenko and Goodier [52] and Bathe and Chaudhary [53].

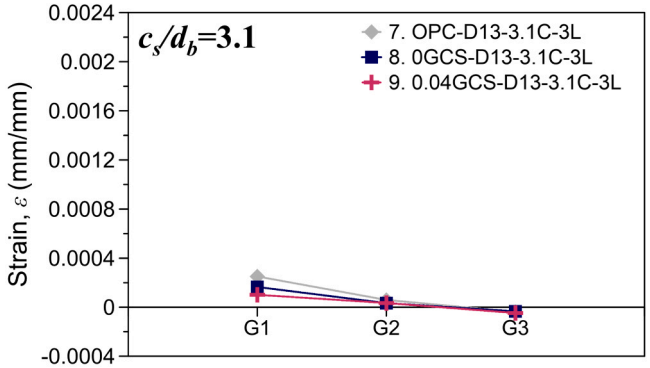

(a) c_s/d_b=3.1

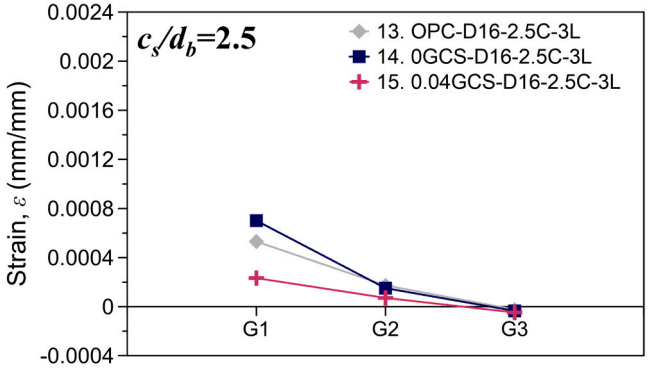

(b) c_s/d_b=2.5

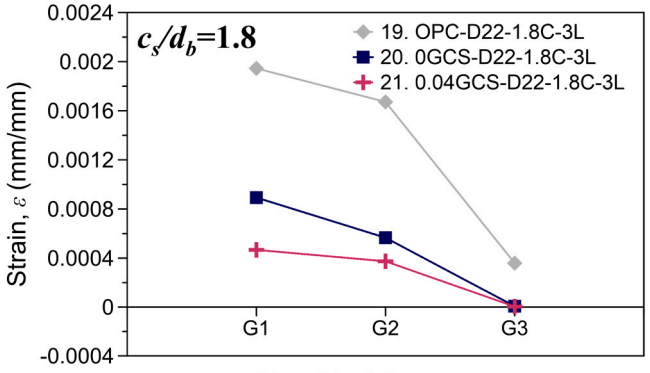

(c) c_s/d_b=1.8

Fig. 12. Concrete strain at maximum load.

$$\tau_f = \frac{R_s \varepsilon_{sh} E_s'}{2 l_d \upsilon_s'} \left\{ 1 - \exp\left[- \frac{2\mu l_d \upsilon_s' \left(1 - \left(\frac{R_s}{R_c} \right)^2 \right)}{\left\{ (1-\upsilon_s') \left(1 - \left(\frac{R_s}{R_c} \right)^2 \right) + \frac{E_s'}{E_c'} \left[(1+\upsilon_c') - \left(\frac{R_s}{R_c} \right)^2 (1-\upsilon_c') \right] \right\} R_s} \right] \right\} \tag{8}$$

Here, ε_{sh} is concrete shrinkage, μ is friction coefficient, E_s is elastic modulus of reinforcing bars, υ_s is Poisson's ratio of reinforcing bar, $E_s^{'} = E_s/(1-\upsilon_s^2)$, $E_c^{'} = E_c/(1-\upsilon_c^2)$, $\upsilon_s^{'} = \upsilon_s/(1-\upsilon_s)$, $\upsilon_c^{'} = \upsilon_c/(1-\upsilon_c)$, and $R_c = R_s + c_s$.

In the *fib* ModelCode 2010 [47], it is stated that the direct tensile strength f_{ct} has the same value as the splitting tensile strength f_{sp}. Therefore, in this study, f_{sp} was used instead of f_{ct}. Therefore, τ_{sp} is calculated as in Eq. (9).

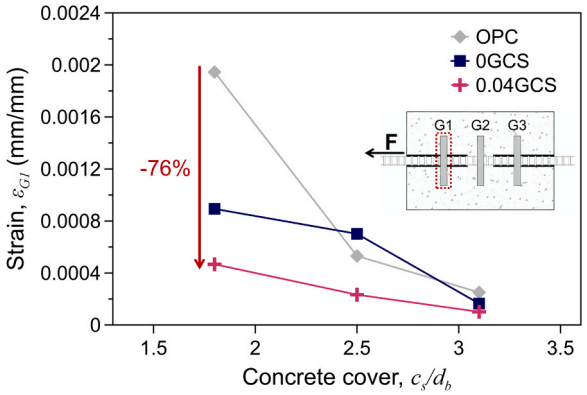

Fig. 13. Effect of concrete cover on concrete strain.

$$\tau_{sp} = f_{sp}\frac{c_s + R_s}{1.664d_b} + \frac{R_s\varepsilon_{sh}E_s'}{2l_d\upsilon_s'}\left\{1 - \exp\left[-\frac{2\mu l_d\upsilon_s'\left(1-\left(\frac{R_s}{R_c}\right)^2\right)}{\left\{(1-\upsilon_s')\left(1-\left(\frac{R_s}{R_c}\right)^2\right) + \frac{E_s'}{E_c'}\left[(1+\upsilon_c') - \left(\frac{R_s}{R_c}\right)^2(1-\upsilon_c')\right]\right\}R_s}\right]\right\} \quad (9)$$

To incorporate the mechanical properties of concrete for each mixture, the values of E_c and υ_c from Table 4 were substituted into Eq. (9). In addition, 1.05 suggested by Allwood and Abullah [54] for μ and 0.00800 suggested by Wight [55] for ε_{sh} were substituted into Eq. (9). Table 8 shows the results calculated using Eq. (9). In addition, Fig. 14 is a graph showing a comparison of the calculated value and the test results. The calculated value (τ_{calc}) of the specimen using OPC and 0.04GCS concrete has an error of approximately 5 % when compared with the test results. Therefore, τ_{calc} accurately predicts the actual bond strength. However, τ_{calc} of the specimen using 0GCS were overestimated by about 18 % compared to the test results. This is because the non-incorporation of GO lowered the dispersion of the solution, resulting in agglomeration.

In future studies, μ and ε_{sh} of triple hybrid-reinforced concrete should be measured to more accurately predict the bond strength of triple hybrid-reinforced concrete. Additionally, factors such as surface angle of the crushed concrete and rib face angle affect radial stress should be explored to predict the bond strength more accurately.

5. Conclusions

The purpose of this study was to evaluate the bond strength considering the mechanical properties of triple hybrid-reinforced concrete. The pull-out test was conducted on a total of 21 specimens, and the following conclusions were obtained.

(1) When nanomaterials were incorporated into concrete, there was no significant difference in compressive strength. Conversely, the splitting tensile strength was increased compared to OPC. 0GCS without GO increased by about 6.4 % compared to OPC, and

Table 8
Results of calculated and experimental bond strength.

No.	Specimen	Failure mode	τ_{calc} (MPa)	$\tau_{b,max}$ (MPa)	$\tau_{calc}/\tau_{b,max}$	Average of $\tau_{calc}/\tau_{b,max}$	Coefficient of variation
7	OPC-D13-3.1C-3L	Splitting	28.38	28.34	1.00	0.95	0.11
10	OPC-D16-5.8C-3L		36.73	43.53	0.84		
13	OPC-D16-2.5C-3L		26.49	29.43	0.90		
16	OPC-D22-4.5C-3L		33.53	30.58	1.10		
19	OPC-D22-1.8C-3L		24.74	27.51	0.90		
5	0GCS-D13-7.4C-3L		46.03	47.23	0.97	1.18	0.22
8	0GCS-D13-3.1C-3L		30.85	25.19	1.22		
14	0GCS-D16-2.5C-3L		28.70	26.49	1.08		
17	0GCS-D22-4.5C-3L		33.64	20.84	1.61		
20	0GCS-D22-1.8C-3L		24.49	24.65	0.99		
9	0.04GCS-D13-3.1C-3L		31.71	34.52	0.92	0.94	0.14
12	0.04GCS-D16-5.8C-3L		34.64	47.16	0.73		
15	0.04GCS-D16-2.5C-3L		25.85	25.72	1.00		
18	0.04GCS-D22-4.5C-3L		31.55	33.00	0.96		
21	0.04GCS-D22-1.8C-3L		23.33	21.23	1.10		

τ_{calc}: calculated bond strength.

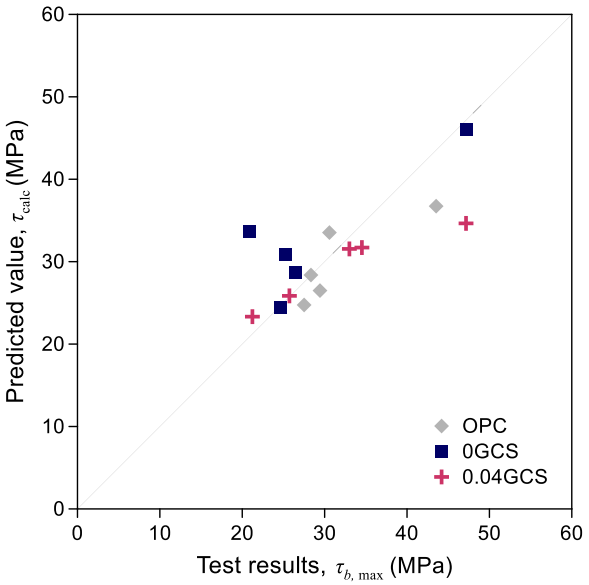

Fig. 14. Evaluation of bond strength predictions.

0.04GCS mixed with GO increased by about 31.0 % compared to OPC. Poisson's ratio and volumetric strain were the lowest at 0.04GCS. In particular, the volumetric strain of 0.04GCS was reduced by about 33.7 % compared to OPC, which had the largest volumetric strain.

(2) As a result of pull-out tests, it showed that slip decreased according to GO incorporation. As for the increase in $\tau_{b,\max}/f_{sp}$ according to c_s/d_b, 0.04GCS was the highest at 1.14. The strain generated in the specimen during the pull-out test was the smallest in the specimen using 0.04GCS concrete regardless of the concrete cover. The specimens using 0.04 GCS concrete showed reduced strain by up to 76 % compared to OPC. This is a result reflects the mechanical properties of 0.04 GCS, which had the smallest Poisson's ratio and volumetric strain.

(3) Calculations considering the mechanical properties of concrete in the formula for splitting bond strength showed that the error between the calculated value and the experimental value for OPC and 0.04GCS was around 5 %. On the other hand, the calculated value of 0GCS was overestimated by about 18 % compared to the test result. This is because GO is not incorporated into 0GCS, which causes agglomeration between nanomaterials.

(4) In this study, the bond strength for various variables was evaluated using the pull-out test, and a methodology for assessing the bond strength of nano-concrete based on its mechanical properties was proposed. However, the validated data relies solely on the limited experiments conducted in this study, which emphasizes the need for further validation using a larger dataset from other studies. Moreover, the pull-out test is an experimental method that overestimates the bond strength. Therefore, in future studies, it is necessary to perform a lap splice test on reinforced concrete beams to determine appropriate design lengths.

Declaration of Competing Interest

The authors declare the following financial interests/personal relationships which may be considered as potential competing interests: Chang-Sik Choi reports financial support was provided by National Research Foundation of Korea.

Data Availability

The data that has been used is confidential.

Acknowledgement

This research was supported by the Basic Science Research Program through the National Research Foundation of Korea (NRF) funded by the Ministry of Education (RS-2023-00207763).

References

[1] C.D. Atiş, O. Karahan, Properties of steel fiber reinforced fly ash concrete, Constr. Build. Mater. 23 (1) (2009) 392–399.
[2] A. Bentur, S. Mindess, Fibre Reinforced Cementitious Composites, Crc Press, 2006.
[3] J. Cao, D. Chung, Improving the dispersion of steel fibers in cement mortar by the addition of silane, Cem. Concr. Res. 31 (2) (2001) 309–311.

[4] M.M. Norhasri, M. Hamidah, A.M. Fadzil, Applications of using nano material in concrete: a review, Constr. Build. Mater. 133 (2017) 91–97.
[5] M. Metaxa, S. Konsta-Gdoutos, Shah, Carbon nanotubes reinforced concrete, Spec. Publ. 267 (2009) 11–20.
[6] A. Carriço, J. Bogas, A. Hawreen, M. Guedes, Durability of multi-walled carbon nanotube reinforced concrete, Constr. Build. Mater. 164 (2018) 121–133.
[7] M. Amin, K. Abu el-Hassan, Effect of using different types of nano materials on mechanical properties of high strength concrete, Constr. Build. Mater. 80 (2015) 116–124.
[8] A. Khaloo, M.H. Mobini, P. Hosseini, Influence of different types of nano-SiO2 particles on properties of high-performance concrete, Constr. Build. Mater. 113 (2016) 188–201.
[9] L. Raki, J. Beaudoin, R. Alizadeh, J. Makar, T. Sato, Cement and concrete nanoscience and nanotechnology, Materials 3 (2) (2010) 918–942.
[10] J. Silvestre, N. Silvestre, J. De Brito, Brito, Review on concrete nanotechnology, Eur. J. Environ. Civ. Eng. 20 (4) (2016) 455–485.
[11] Z. Lu, D. Hou, L. Meng, G. Sun, C. Lu, Z. Li, Mechanism of cement paste reinforced by graphene oxide/carbon nanotubes composites with enhanced mechanical properties, RSC Adv. 5 (122) (2015) 100598–100605.
[12] M.O. Mohsen, M.S. Al Ansari, R. Taha, N. Al Nuaimi, A.A. Taqa, Carbon nanotube effect on the ductility, flexural strength, and permeability of concrete, J. Nanomater. 2019 (2019) 1–11.
[13] Y. Murad, Compressive strength prediction for concrete modified with nanomaterials, Case Stud. Constr. Mater. 15 (2021), e00660.
[14] S. Xu, J. Liu, Q. Li, Mechanical properties and microstructure of multi-walled carbon nanotube-reinforced cement paste, Constr. Build. Mater. 76 (2015) 16–23.
[15] H. Du, S. Du, X. Liu, Durability performances of concrete with nano-silica, Constr. Build. Mater. 73 (2014) 705–712.
[16] M.H. Beigi, J. Berenjian, O.L. Omran, A.S. Nik, I.M. Nikbin, An experimental survey on combined effects of fibers and nanosilica on the mechanical, rheological, and durability properties of self-compacting concrete, Mater. Des. 50 (2013) 1019–1029.
[17] S. Chuah, Z. Pan, J.G. Sanjayan, C.M. Wang, W.H. Duan, Nano reinforced cement and concrete composites and new perspective from graphene oxide, Constr. Build. Mater. 73 (2014) 113–124.
[18] G. Kim, H. Suh, S. Cho, S. Im, E.Z. Nezhad, S. Seok, C. Choi, S. Bae, Synergistic strengthening mechanism of Portland cement paste reinforced by a triple hybrid of graphene oxide, functionalized carbon nanotube, and nano-silica, Constr. Build. Mater. 352 (2022), 129017.
[19] D.-H. Son, D. Hwangbo, H. Suh, B.-I. Bae, S. Bae, C.-S. Choi, Mechanical properties of mortar and concrete incorporated with concentrated graphene oxide, functionalized carbon nanotube, nano silica hybrid aqueous solution, Case Stud. Constr. Mater. 18 (2023), e01603.
[20] L.A. Lutz, P. Gergely, Mechanics of bond and slip of deformed bars in concrete, J. Proc. (1967) 711–721.
[21] R. Tepfers, Cracking of concrete cover along anchored deformed reinforcing bars, Mag. Concr. Res. 31 (106) (1979) 3–12.
[22] M.R. Esfahani, B.V. Rangan, Local bond strength of reinforcing bars in normal strength and high-strength concrete (HSC), Struct. J. 95 (2) (1998) 96–106.
[23] R. Tepfers, A Theory of Bond Applied to Overlapped Tensile Reinforcement Splices for Deformed Bars, Chalmers University of Technology, Goteborg, Sweden, 1973.
[24] T. Tilanterä, T. Rechardt, A. Solodovnik, G. Kunnos, R. Johanson, Bond of reinforcement in lightweight aggregate concrete, Tek. Korkeak. (1977).
[25] L.J. Hou, R. Xu, Y.P. Zang, F. Ouyang, D. Chen, L. Zhong, Bond behavior between reinforcement and ultra-high toughness cementitious composite in flexural members, Eng. Struct. 210 (2020), 110357.
[26] B.I. Bae, H.K. Choi, C.S. Choi, Bond stress between conventional reinforcement and steel fibre reinforced reactive powder concrete, Constr. Build. Mater. 112 (2016) 825–835.
[27] X. Wang, S. Dong, A. Ashour, S. Ding, B. Han, Bond behaviors between nano-engineered concrete and steel bars, Constr. Build. Mater. 299 (2021), 124261.
[28] A. Hassan, H. Elkady, I.G. Shaaban, Effect of adding carbon nanotubes on corrosion rates and steel-concrete bond, Sci. Rep. 9 (1) (2019) 6285.
[29] A. Hawreen, J. Bogas, Influence of carbon nanotubes on steel–concrete bond strength, Mater. Struct. 51 (2018) 1–16.
[30] X. Wang, S. Ding, L. Qiu, A. Ashour, Y. Wang, B. Han, J. Ou, Improving bond of fiber-reinforced polymer bars with concrete through incorporating nanomaterials, Compos. Part B: Eng. 239 (2022), 109960.
[31] M. Alhawat, A. Ashour, Bond strength between corroded steel and recycled aggregate concrete incorporating nano silica, Constr. Build. Mater. 237 (2020), 117441.
[32] S.S. Mousavi, S.S.M. Ajarostaghi, C. Bhojaraju, A critical review of the effect of concrete composition on rebar-concrete interface (RCI) bond strength: a case study of nanoparticles, SN Appl. Sci. 2 (5) (2020) 893.
[33] Y. Charonnat, H. Beitzel, Report: efficiency of concrete mixers towards qualification of mixers, Mater. Struct. 30 (1997) 28–32.
[34] KS F 2405, Standard test method for compressive strength of concrete. Korean Standard Information Center, 2010.
[35] KS F 2423, Standard Test Method for Tensile Splitting Strength of Concrete. Korean Standard Information Center, 2021.
[36] KS F 2438, Standard test method for static modulus of elasticity and Poisson's ratio in compression of cylindrical concrete specimens. Korean Standard Information Center, 2017.
[37] ACI Committee 408, in: Bond and Development of Straight Reinforcing Bars in Tension (ACI 408R-03) (Reapproved 2012), American Concrete Institute, Farmington Hills, MI, 2003, p. 49.
[38] D. Darwin, J. Zuo, M.L. Tholen, E.K. Idun, Development Length Criteria for Conventional and High Relative Rib Area Reinforcing Bars, University of Kansas Center for Research, Inc, 1995.
[39] Ve.A. Veljkovic, V. Carvelli, M.M. Haffke, M. Pahn, Concrete cover effect on the bond of GFRP bar and concrete under static loading, Compos. Part B: Eng. 124 (2017) 40–53.
[40] I. Pop, G. De Schutter, P. Desnerck, T. Onet, Bond between powder type self-compacting concrete and steel reinforcement, Constr. Build. Mater. 41 (2013) 824–833.
[41] ACI Committee 318, Building Code Requirements for Structural Concrete (ACI 318–19) and Commentary, American Concrete Institute, Farmington Hills, MI, 2019.
[42] RILEM. RC6: Bond test for reinforcing steel. 1: Pull-out text. RILEM technical recommendations for the testing and use of construction materials, E & FN Spon, London, 1994b, pp. 102–105.
[43] KDS 14 20 52: 2021, Korea Ministry of Land, Infrastructure and Transpor, 2021.
[44] KS B 0802, Method of Tensile Test for Metallic Materials, Korean Standard Information Center, 2013.
[45] W. Wei, F. Liu, Z. Xiong, Z.Y. Lu, L.J. Li, Bond performance between fibre-reinforced polymer bars and concrete under pull-out tests, Constr. Build. Mater. 227 (2019), 116803.
[46] R. Okelo, R.L. Yuan, Bond strength of fiber reinforced polymer rebars in normal strength concrete, J. Compos Constr. 9 (3) (2005) 203–213.
[47] CEB-FIP Model Code 2010, Fib Model Code for Concrete Structures 2010, Ernst & Sohn, Wiley, Berlin, Germany, 2013.
[48] G. Rehm, The fundamental law of bond, in: Proceedings of the Symposium on Bond and Crack Formation in Reinforced Concrete, Stockholm, 1957, pp. 491–498.
[49] L.A. Lutz, The Mechanics of Bond and Slip of Deformed Reinforcing Bars in Concrete, Ph.D. dissertation, Cornell University, 1966.
[50] KS D 3504, Steel Bars for Concrete Reinforcement, Korean Standard Information Center, 2021.
[51] A. Hu, X. Liang, Q. Shi, Bond characteristics between high-strength bars and ultrahigh-performance concrete, J. Mater. Civ. Eng. 32 (1) (2020), 04019323.
[52] S. Timoshenko, J.N. Goodier. Theory of Elasticity, 3 ed., McGraw-Hill, 1951.
[53] K.J. Bathe, A. Chaudhary, A solution method for planar and axisymmetric contact problems, Int. J. Numer. Methods Eng. 21 (1) (1985) 65–88.
[54] R. Allwood, A.A. Bajarwan, Modeling nonlinear bond-slip behavior for finite element analyses of reinforced concrete structures, Struct. J. 93 (5) (1996) 538–544.
[55] J.G. MacGregor, J.K. Wight, S. Teng, P. Irawan, Reinforced Concrete: Mechanics and Design, Prentice Hall Upper, Saddle River, NJ, 1997.